Polymer Journal
https://doi.org/10.1038/s41428-024-00912-x

ORIGINAL ARTICLE

Effect of polymer concentration on molecular alignment behavior during scanning wave photopolymerization

Takuto Ishiyama[1,2] · Yoshiaki Kobayashi[1,2] · Hirona Nakamura[1,2] · Miho Aizawa[1,2,3] · Kyohei Hisano[1,2] · Shoichi Kubo[1,2] · Atsushi Shishido[1,2,4]

Received: 27 January 2024 / Revised: 17 March 2024 / Accepted: 1 April 2024

Abstract

Molecularly aligned liquid-crystalline (LC) polymer films hold great promise for next-generation high-performance photonics, electronics, robotics, and medical devices. Photoalignment methods capable of achieving precise molecular alignment in a noncontact manner have been actively studied. Recently, we proposed the concept of using spatiotemporal photopolymerization to induce molecular diffusion and the resulting alignment, termed scanning wave photopolymerization (SWaP). The spatial gradient of the polymer concentration is the dominant factor in inducing the molecular diffusion and alignment of LCs. However, the effect of polymer concentration on molecular alignment behavior remains unclear. In this study, we performed SWaP at different exposure energies to modulate the polymer concentration during polymerization. We found that a certain polymer concentration was required to initiate the alignment. Furthermore, the phase diagram of the polymer/monomer mixtures and real-time observations during SWaP revealed that phase emergence and unidirectional molecular alignment occurred simultaneously when the polymer concentration exceeded 50%. Since SWaP achieves molecular alignment coincident with photopolymerization, it has the potential to revolutionize material fabrication by consolidating the multiple-step processes required to create functional materials in a single step.

Introduction

Precise control of molecular alignment is crucial because it enables the amplification of molecular functionality to the macroscopic level, which substantially enhances the various properties of materials [1–4]. Materials fabricated with controlled molecular alignment are expected to find applications in the next generation of high-performance optics [5, 6], electronics [7, 8], robotics [9, 10], and medical devices [11, 12]. One key material is liquid crystals (LCs), which exhibit various anisotropic properties due to their molecular alignability based on their cooperative effect. Among the various techniques proposed for aligning LCs over large areas, mechanical methods are commonly used industrially to induce macroscopic molecular alignment [13–15]. Representative examples include the stretching of LC polymer films and the coating of LCs over a rubbed surface. These methods are highly convenient and powerful for inducing unidirectional alignment; however, they involve possible damage to materials due to their contact-based nature. In addition, precise alignment control is inherently difficult with two or more dimensions. Photoalignment techniques with the advantages of a noncontact process and high spatial resolution have been explored as alternatives [16–26]. The photoalignment method was first reported by Ichimura et al. [17]. Nematic LCs on an azobenzene monolayer reversibly change their alignment direction through *trans–cis* photoisomerization of

Supplementary information The online version contains supplementary material available at https://doi.org/10.1038/s41428-024-00912-x.

✉ Atsushi Shishido
ashishid@res.titech.ac.jp

[1] Laboratory for Chemistry and Life Science, Institute of Innovative Research, Tokyo Institute of Technology, 4259 Nagatsuta, Midori-ku, Yokohama 226-8501, Japan

[2] Department of Chemical Science and Engineering, School of Materials and Chemical Technology, Tokyo Institute of Technology, 2-12-1 Ookayama, Meguro-ku, Tokyo 152-8552, Japan

[3] PRESTO, JST, 4-1-8 Honcho, Kawaguchi 332-0012, Japan

[4] Research Center for Autonomous Systems Materialogy, Institute of Innovative Research, Tokyo Institute of Technology, 4259 Nagatsuta, Midori-ku, Yokohama 226-8501, Japan

Published online: 23 April 2024

azobenzenes [17]. In addition to the *trans–cis* photoisomerization of azobenzenes [18, 19], other photoalignment methods utilizing different photochemical reaction systems, including the photocrosslinking of cinnamate derivatives [20–22], the photo-Fries rearrangement of phenyl benzoate derivatives [23, 24], and the photodecomposition of polyimides [25, 26], have been reported. The advancement of such photoalignment methods has enabled precise two-dimensional alignment and facilitated the fabrication of advanced materials for applications such as holograms [27–29], solar cells [30], and soft actuators [9, 10, 31, 32].

Recently, we proposed a new concept of a photoalignment process, termed scanning wave photopolymerization (SWaP), where spatiotemporal photopolymerization induces molecular diffusion, acting as the driving force for aligning molecules [33–38]. Spatio-selective photopolymerization produces polymers only in the irradiated region, causing the concentration gradients of monomers and polymers at the boundary between the irradiated and unirradiated regions. Mutual molecular diffusion occurs at the boundary to compensate for this spatial difference in the concentration, resulting in the alignment of anisotropic molecules along the diffusion direction. Light scanning generates steady-state molecular diffusion and aligns molecules over a large area. Since SWaP utilizes physicochemical phenomenon, i.e., molecular diffusion, as the driving force for alignment, it enables precise control of alignment in various materials and polymerization systems in terms of mesogen structures [33], guest dye molecules [35], additive polymers [33], and radical and cationic polymerization systems [33]. Moreover, various one- and two-dimensional alignment patterns over a large area were induced simply by changing the shape and movement of irradiation light patterns [33, 35, 36]. To elucidate the underlying mechanism, we conducted a series of experiments on the effects of the film thickness [33], polymerization temperature [33], light scanning rate [33], and LC phase on the alignment behavior [38]. Furthermore, we performed theoretical calculations [33] and visualized molecular diffusion using quantum dots [37]. The spatial distribution of the polymer concentration is the dominant factor in molecular diffusion and the resulting alignment of LCs. However, the effect of polymer concentration on the molecular alignment behavior during SWaP has yet to be explored. In this study, we performed SWaP under different exposure energies to modulate spatiotemporal polymer concentrations and investigated their molecular alignment behavior. We found that a certain exposure dose during SWaP was required to induce unidirectional molecular alignment over large areas. Furthermore, a phase diagram of the polymer/monomer mixtures and real-time observation of the SWaP process using a polarized optical microscope revealed that an LC phase emerged when the polymer concentration exceeded the threshold value, and the molecular alignment was stabilized. This underlying mechanism suggests that SWaP enables dynamic control of photopolymerization and molecular alignment. This finding demonstrates the innovative aspect of SWaP, by which the entire process of polymer synthesis, alignment, and film formation can be conducted in a single light irradiation step, avoiding time-consuming and labor-intensive processes.

Experimental procedures

Materials

The chemical structures of the materials used in this study are shown in Fig. 1. The photopolymerizable anisotropic monomer 4-cyanophenyl 4-((6-(methacryloyloxy)hexyl) oxy)benzoate (M6BACP) was obtained from ENEOS Corp., Tokyo, Japan. The photoinitiator Irgacure 651 was purchased from Tokyo Chemical Industry Co., Ltd., Tokyo, Japan. Unless otherwise stated, the compounds were used without any purification.

Fabrication of polymer films by SWaP

Two types of glass cells were prepared for photopolymerization according to the irradiation setup: one used two glass substrates with a size of 25 × 15 mm, and the other consisted of a glass substrate (25 × 25 mm) and a micro cover glass (18 × 18 mm). The glass substrates were ultrasonically cleaned with 2-propanol for 30 min before use. The gap of the glass cells was determined by bonding with glue containing 2-μm-diameter silica spacers (Thermo Scientific, 9000 Series, #9002, Thermo Fisher Scientific, Waltham, MA, USA). A glass cell fabricated with a microcover glass was used for in situ observation during SWaP.

A schematic illustration of the photopolymerization of M6BACP by SWaP is shown in Fig. 2. A polymerizable sample was prepared by mixing M6BACP and Irgacure 651 at a molar ratio of 100:1, following the procedure described in our previous study [33], and was injected into glass cells by melting at 150 °C. After cooling to 90 °C, at which point the polymerized M6BACP exhibited an LC phase, the sample was irradiated with a scanned ultraviolet (UV) slit light using a UV–digital light processor (UV–DLP;

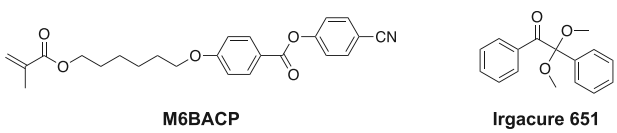

Fig. 1 Chemical structures of the materials used in this study

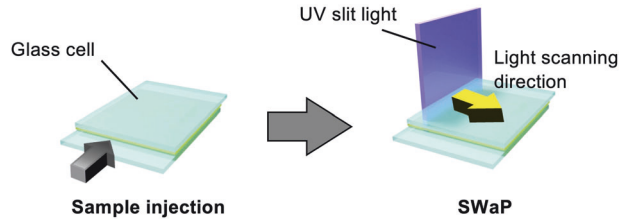

Fig. 2 Schematic illustrations of the photopolymerization process with scanned slit light

MLS-DIR-LC65365, ASKA Corp., Japan) to initiate photopolymerization. For the in situ observation during SWaP, an irradiation setup was designed to incorporate a DLP within a polarized optical microscope (POM; BX53, Olympus Co., Ltd., Japan), termed POM–DLP (MLS-OLBX-LC45365, ASKA Corp., Japan). The DLP employed both in UV–DLP and POM–DLP consists of a digital micromirror device (DMD) and a UV light-emitting diode (LED) with a peak wavelength of 369 nm for UV–DLP and 374 nm for POM–DLP. The DMD pixel size is 7.56 µm square at 1920 × 1080 pixels for UV–DLP and 5.40 µm square at 1280 × 720 pixels for POM–DLP. In POM–DLP, a longpass filter (R-62, AGC Techno Glass Co., Ltd., Japan) was installed at the light source of POM to prevent the progress of polymerization caused by exposure other than the UV–LED. After photopolymerization, the cell was immersed in liquid nitrogen and quenched to room temperature to obtain a polymer film.

Evaluation of molecular alignment

The optical anisotropy and molecular alignment of the obtained polymer films were evaluated by using POM equipped with a Berek compensator (U-CBE, Olympus Corp., Tokyo, Japan). The birefringence (Δn) was evaluated by measuring the retardation (R) and dividing R by the film thickness (d) according to the equation $\Delta n = R/d$ [39].

Evaluation of the LC properties of the M6BACP monomer and polymer mixtures

M6BACP polymers were prepared by the following procedure. The polymerizable sample was injected into a glass cell made by bonding two glass substrates (25 × 75 mm) with a 100-µm-thick polyimide spacer at 150 °C and cooled to 90 °C. Polymerization was conducted by irradiation with 365 nm UV light throughout the cell at an intensity of 15 mW/cm^2 for 30 min by a UV–LED (LHPUV365-2501, Iwasaki Electric Co., Ltd., Japan). The ^{1}H NMR spectrum and molecular weight distribution curve of the polymer revealed a number-average molecular weight of 109,900, a polydispersity index of 2.4, and a conversion of 99% (Supplementary Text S1, Supplementary Fig. S3). Samples with various polymer concentrations were prepared by weighing the obtained polymer and monomer separately on a balance and then mixing them to weight fractions of 0–99 wt%. The mixture was dissolved in THF and stirred for 1 day at room temperature. After the solvent was removed under vacuum for 3 h at 40 °C, 1 h at 80 °C, and 8 h at room temperature, the LC properties of the monomer/polymer mixtures were evaluated by differential scanning calorimetry (DSC, DSC7000X, Hitachi High-Tech Corp., Tokyo, Japan) at a scanning rate of 10 °C/min.

Results and discussion

Effect of exposure dose on the molecular alignment behavior of SWaP

The effect of the polymer concentration during SWaP on the degree of molecular alignment was investigated by altering the exposure dose (E) in the SWaP process. The value of E was calculated by using the following equation: $E = w \times I/v$, where I, w, and v represent the light intensity (mW/cm^2), slit width (µm), and light scanning rate (µm/s), respectively. The photoirradiation conditions are summarized in Table 1. The light intensity was fixed at 35 mW/cm^2, and E was adjusted to 1.8–560 mJ/cm^2 by changing the slit width and the light scanning rate. As representative examples, POM images of the polymer films fabricated at E values of 280, 140, and 58 mJ/cm^2 are shown in Fig. 3a–c. The films obtained at E values of 280 and 140 mJ/cm^2 exhibited uniform optical anisotropy; the images were completely dark when the light scanning direction was parallel or perpendicular to the polarizers and became bright when the films were rotated by 45°. Furthermore, POM observation with a Berek compensator revealed that the anisotropic units (phenyl benzoate moieties) were aligned unidirectionally along the light scanning direction (Supplementary Fig. S2). When E was 58 mJ/cm^2, neither uniform optical anisotropy nor unidirectional molecular alignment was induced. To quantify the degree of molecular alignment, the birefringence (Δn) of the polymer films fabricated under various exposure doses was evaluated (Fig. 2d, Supplementary Table S1). The films fabricated at exposure doses of 58 mJ/cm^2 or less showed no optical anisotropy, which indicates that the molecular alignment was macroscopically random. In contrast, unidirectional molecular alignment was induced above 140 mJ/cm^2, with a maximum Δn of 0.04 at 280 mJ/cm^2. An increase in the exposure dose yields a greater polymer concentration in the films, suggesting that a certain polymer concentration is required to align molecules in SWaP.

Phase diagram of M6BACP polymer/monomer mixtures

The polymer concentration dependence of the molecular alignment behavior may be related to the LC phase of the polymer/monomer mixture. The difference in the LC-to-isotropic phase transition temperature due to the polymer concentration in the mixture may cause a dynamic change in the phase during SWaP and affect the molecular alignment behavior. As a first step in exploring the potential influence of the LC phase on molecular alignment induction, the relationship between the polymer concentration and the LC phase was investigated. Figure 4a shows DSC thermograms of the polymer/monomer mixtures with various polymer concentrations. The homopolymer (polymer concentration of 99%) showed an exothermic peak at 117 °C. POM observation under crossed polarizers of the homopolymer below 117 °C showed a schlieren texture characteristic of an LC phase, which became completely dark above 117 °C (Fig. 4b). Therefore, the exothermic peak is attributed to an LC-isotropic phase transition. These results are consistent with previous reports [40]. On the other hand, the monomer (polymer concentration of 0%) showed an exothermic peak at 30 °C. POM observation revealed that the peak is derived from a crystalline-isotropic phase transition without showing an LC phase (Fig. 4c).

Table 1 Photoirradiation conditions for SWaP

Entry	Light intensity (mW/cm^2)	Slit width (μm)	Scanning rate (μm/s)	Exposure dose (mJ/cm^2)
1	35	5.2	99	1.8
2	35	5.2	78	2.3
3	35	5.2	62	3.2
4	35	5.2	31	5.8
5	35	28	31	29
6	35	52	31	58
7	35	125	31	140
8	35	250	31	280
9	35	500	31	560

The polymer/monomer mixtures at polymer concentrations between 99 and 20% showed a single exothermic peak derived from the LC-isotropic phase transition. POM observation of the mixtures also revealed the presence of the LC phase (Supplementary Fig. S4). With decreasing polymer concentration, the phase transition temperature decreased from 117 to 61 °C. The mixture with a polymer concentration of 10% showed two exothermic peaks. The high-temperature side (red triangle) and the low-temperature side (purple triangle) were attributed to LC-isotropic and crystalline-LC phase transitions, respectively. A phase diagram of the M6BACP polymer/monomer mixture is shown to summarize the phase transition temperatures (Fig. 5). The diagram clearly indicates that the temperature range in which the LC phase shifts toward higher temperatures as the polymer concentration increases. Focusing on the phase transition behavior during SWaP conducted at 90 °C, it was revealed that the LC phase appeared at a polymer concentration higher than 50%.

Real-time observation of the molecular alignment induced by SWaP

To understand the emergence of the LC phase during SWaP and its influence on molecular alignment behavior, real-time observation of molecular alignment during SWaP was carried out by employing POM–DLP. The SWaP was conducted with a light intensity of 35 mW/cm^2, a light scanning rate of 31 μm/s, exposure doses of 29, 280, and 560 mJ/cm^2, and slit widths of 26, 250, and 501 μm. Snapshots of the POM observations during SWaP are shown in Fig. 6 (see Supplementary Movies 1–3). At an exposure dose of 29 mJ/cm^2, no bright region was observed in the area immediately after the slit light passed, implying that the LC phase did not appear during the polymerization process with the scanned slit light (Fig. 6a). A bright region indicating the emergence of the LC phase appeared after 93 s and expanded throughout the whole area at 106 s, macroscopically revealing a typical polydomain structure without uniform optical anisotropy. On the other hand, at exposure energies of 280 and 560 mJ/cm^2, the LC phase appeared at

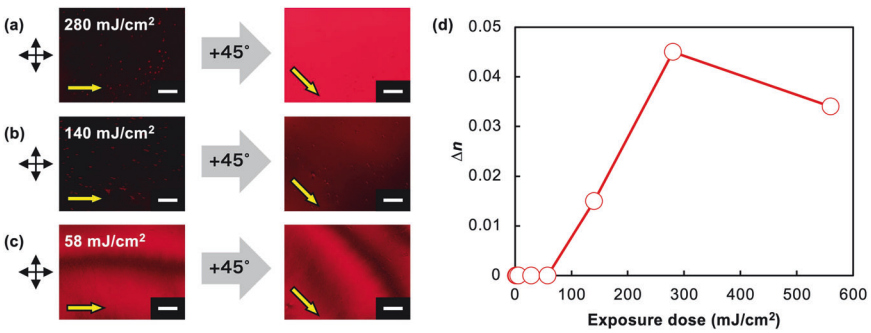

Fig. 3 POM images of the polymer films fabricated by SWaP at exposure doses of 280 mJ/cm^2 (**a**), 140 mJ/cm^2 (**b**), and 58 mJ/cm^2 (**c**). The crossed arrows show the direction of the polarizers. Yellow arrows show the light scanning direction. Scale bars, 200 μm. **d** Birefringence of the polymer films obtained by SWaP as a function of exposure dose

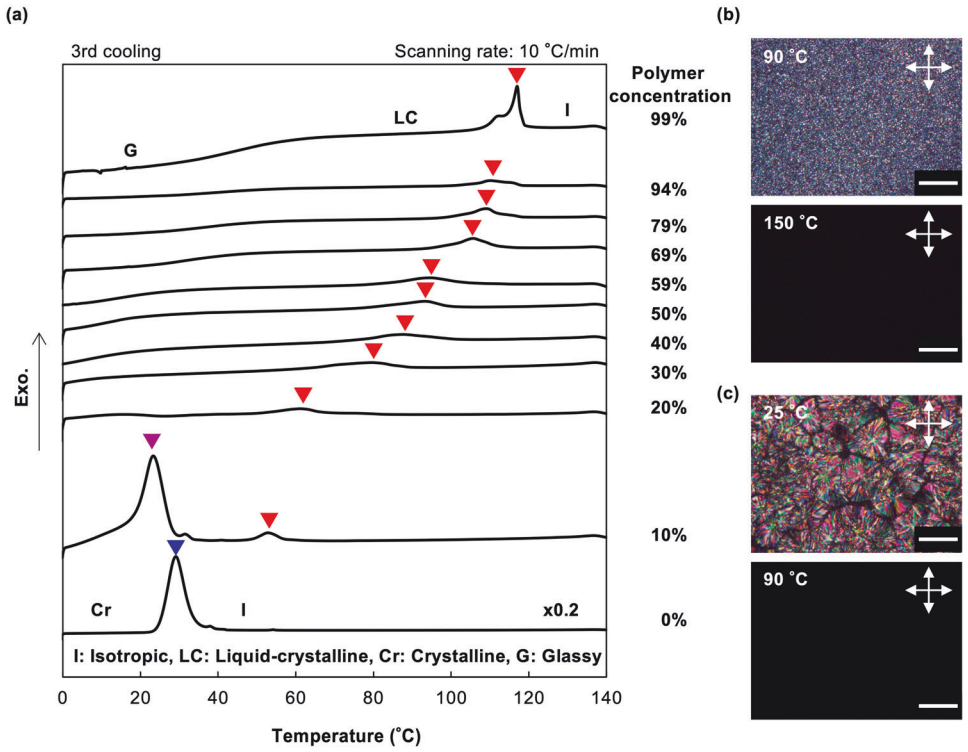

Fig. 4 **a** DSC thermograms of the polymer/monomer mixtures with polymer concentrations of 0–99% during the third cooling process at a scan rate of 10 °C/min. Red, blue, and purple triangles show the temperatures of the LC–isotropic, crystalline–isotropic, and crystalline–LC phase transitions, respectively. POM images of the homopolymer (**b**) and monomer (**c**) films. The observed temperatures of the films are depicted in the images. The crossed arrows show the direction of the polarizers. Scale bars: 20 µm

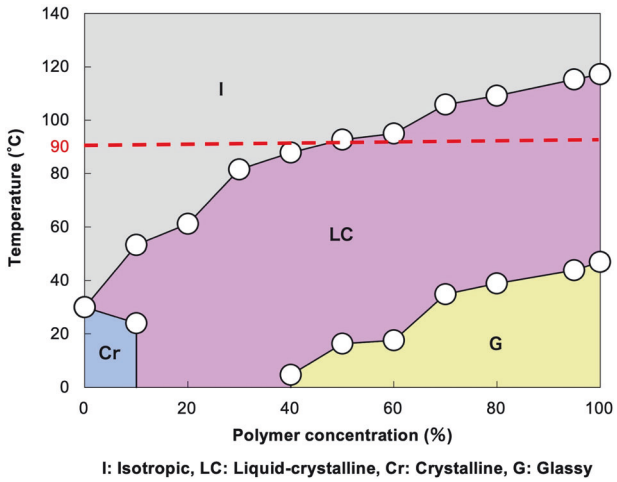

Fig. 5 Phase diagram of the mixture of the M6BACP polymer and monomer. The gray, pink, blue, and yellow areas represent the isotropic, LC, crystalline phases, and glassy state, respectively

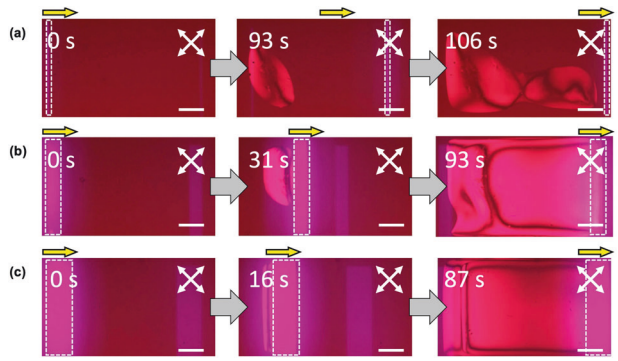

Fig. 6 Snapshots of real-time observation using POM–DLP during SWaP at exposure doses of 29 mJ/cm^2 (**a**), 280 mJ/cm^2 (**b**), and 560 mJ/cm^2 (**c**). POM images were taken at 0, 93, and 106 s (**a**); 0, 31, and 93 s (**b**); and 0, 16, and 87 s (**c**) after starting irradiation. The white dashed squares show the irradiated areas. The crossed arrows show the direction of the polarizer. Yellow arrows show the light scanning direction. Scale bars: 500 µm

31 and 16 s, respectively, upon the passage of the slit light (Fig. 6b, c). This indicates that these exposure energies are sufficient to bring about a polymer concentration above 50%, which is necessary for the emergence of the LC phase at 90 °C. The observed LC phase regions showed uniform optical anisotropy with unidirectional molecular alignment under these conditions. Therefore, we concluded that SWaP caused an increase in the polymer concentration and induced molecular alignment simultaneously with the appearance of the LC phase.

According to the results above, the underlying mechanism of the molecular alignment induced by SWaP can be described as follows. Before polymerization, non-LC monomers are present in a random alignment. SWaP produces polymers only in the irradiated area, and the polymer concentration gradient between the irradiated and unirradiated areas causes mutual molecular diffusion of monomers and polymers. This diffusion causes shear stress on the anisotropic monomers and polymers, resulting in unidirectional molecular alignment along the diffusion direction. When SWaP is performed above a certain

exposure dose, the polymer concentration exceeds 50% immediately after light irradiation, and the LC phase appears. This LC phase emergence contributes to maintaining the aligned state and the rapid increase in viscosity, which leads to an increase in shear stress acting on the anisotropic molecules (Supplementary Fig. S5). The aligned LC state that appears simultaneously as the slit light passes through is stabilized and expanded over large areas along the light scanning direction. On the other hand, under lower exposure dose conditions, the polymer concentration during the passage of the slit light remains below 50%. As a result, the absence of the LC phase during SWaP results in relaxation of the molecular alignment, leading to no uniform optical anisotropy. These results indicate that the polymer concentration and LC phase during SWaP, in which molecular diffusion occurs, are essential for inducing uniform molecular alignment over large areas.

Following the above mechanism, the polymer concentration and polymerization temperature are the dominant factors affecting the molecular alignment behavior during SWaP. We conducted two proof-of-concept experiments: increasing the polymer concentration beforehand (preexposure) and lowering the polymerization temperature to promote the expression of the LC phase. We performed preexposure throughout the cell at a polymerization temperature of 90 °C and an exposure dose of 210 mJ/cm², followed by SWaP at 58 mJ/cm². As a result, unidirectional molecular alignment was induced even under the SWaP condition, where molecular alignment could not be achieved. The photopolymerization at a lowered temperature of 70 °C also resulted in the formation of unidirectional molecular alignment at an exposure dose of 58 mJ/cm^2 (Supplementary Fig. S6).

Conclusion

We investigated the effect of polymer concentration, the dominant factor in molecular diffusion and LC nature, on the molecular alignment behavior induced by our developed photopolymerization technique, SWaP. The investigation of SWaP at various exposure doses revealed that sufficient doses above a certain threshold are required to induce molecular alignment. We hypothesized that the appearance of the LC phase associated with the polymer concentration affects the alignment behavior. A phase diagram of the polymer/monomer mixtures revealed that the LC phase emerged when the polymer concentration reached 50% during SWaP. Furthermore, real-time observation during SWaP revealed a temporal relationship between the presence of the LC phase and the induction of molecular alignment. These results indicated that the emergence of the LC phase during SWaP is the critical factor in molecular alignment. Notably, SWaP enables a single-step preparation of aligned polymer films, which are conventionally prepared by serial processes of polymer synthesis, orientation control, and film fabrication. Therefore, SWaP has the potential to revolutionize material production by serving as a fundamental technique for the development of groundbreaking functional materials.

Acknowledgements This work was supported by Grants-in-Aid for Scientific Research on Innovative Areas "Molecular Engine" (JSPS KAKENHI grant no. JP18H05422), Grants-in-Aid for Scientific Research (B) (JSPS KAKENHI grant number 22H02128), Grants-in-Aid for Transformative Research Areas (JSPS KAKENHI grant number 22H05046), and JST CREST grant no. JPMJCR18I4, Japan. This work was also supported by JST SPRING grant no. JPMJSP2106. This work was performed under the Cooperative Research Program of "Network Joint Research Center for Materials and Devices. This work was performed under the Research Program of the "Dynamic Alliance for Open Innovation Bridging Human, Environment and Materials" and "Crossover Alliance to Create the Future with People, Intelligence and Materials" in the "Network Joint Research Center for Materials and Devices".

Compliance with ethical standards

Conflict of interest The authors declare no competing interests.

Publisher's note Springer Nature remains neutral with regard to jurisdictional claims in published maps and institutional affiliations.

References

1. Uchida J, Soberats B, Gupta M, Kato T. Advanced functional liquid crystals. Adv Mater. 2021;34:2109063.
2. Shishido A. Rewritable holograms based on azobenzene-containing liquid-crystalline polymers. Polym J. 2010;42:525–33.
3. Lakes R. Materials with structural hierarchy. Nature 1993;361:511–15.
4. White TJ, Broer DJ. Programmable and adaptive mechanics with liquid crystal polymer networks and elastomers. Nat Mater. 2015;14:1087–98.
5. Ma LL, Li CY, Pan JT, Ji YE, Jiang C, Zheng R, Wang ZY, Wang Y, Li BX, Lu YQ. Self-assembled liquid crystal architectures for soft matter photonics. Light Sci Appl. 2022;11:270.
6. Bisoyi HK, Li Q. Light-driven liquid crystalline materials: from photo-induced phase transitions and property modulations to applications. Chem Rev. 2016;116:15089–166.
7. O'Neill M, Kelly SM. Liquid crystals for charge transport, luminescence, and photonics. Adv Mater. 2003;15:1135–46.
8. Kim H, Gibson J, Maeng J, Saed MO, Pimentel K, Rihani RT, Pancrazio JJ, Georgakopoulos SV, Ware TH. Responsive, 3D

electronics enabled by liquid crystal elastomer substrates. ACS Appl Mater Interfaces. 2019;11:19506–13.
9. Hebner TS, Bowman RGA, Duffy D, Mostajeran C, Griniasty I, Cohen I, Warner M, Bowman CN, White TJ. Discontinuous metric programming in liquid crystalline elastomers. ACS Appl Mater Interfaces. 2023;15:11092–98.
10. Xiao YY, Jiang ZC, Zhao Y. Liquid crystal polymer-based soft robots. Adv Intell Syst. 2020;2:2000148.
11. Zhang Z, Yang X, Zhao Y, Ye F, Shang L. Liquid crystal materials for biomedical applications. Adv Mater. 2023;35: 2300220.
12. Woltman SJ, Jay GD, Crawford GP. Liquid-crystal materials find a new order in biomedical applications. Nature 2007;6:929–38.
13. Kupfer J, Finkelmann H. Nematic liquid single crystal elastomers. Makromol Rapid Commun. 1991;12:717–26.
14. Berreman DW. Solid surface shape and the alignment of an adjacent nematic liquid crystal. Phys Rev Lett. 1972;28:1683–7.
15. Toney MF, Russell TP, Logan JA, Kikuchi H, Sands JM, Kumar SK. Near-surface alignment of polymers in rubbed films. Nature 1995;374:709–11.
16. Seki T. New strategies and implications for the photoalignment of liquid crystalline polymers. Polym J. 2014;46:751–68.
17. Ichimura K, Suzuki Y, Seki T, Hosoki A, Aoki K. Reversible change in alignment mode of nematic liquid crystals regulated photochemically by "command surfaces" modified with an azobenzene monolayer. Langmuir 1988;4:1214–16.
18. Yaroshchuk O, Reznikov Y. Photoalignment of liquid crystals: basics and current trends. J Mater Chem. 2012;22:286–300.
19. Meier JG, Ruhmann R, Stumpe J. Planar and homeotropic alignment of LC polymers by the combination of photoorientation and self-organization. Macromolecules. 2000;33:843–50.
20. Schadt M, Schmitt K, Kozinkov V, Chigrinov V. Surface-induced parallel alignment of liquid crystals by linearly polymerized photopolymers. Jpn J Appl Phys. 1992;31:2155–64.
21. Kawatsuki N, Hamano K, Ono H, Sasaki T, Goto K. Molecular-oriented photoalignment layer for liquid crystals. Jpn J Appl Phys. 2007;46:339–41.
22. Minami S, Kondo M, Kawatsuki N. Fabrication of UV-inactive photoaligned films by photoinduced orientation of H-bonded composites of non-photoreactive polymer and cinnamate derivative. Polym J. 2016;48:267–71.
23. Kawatsuki N, Neko T, Kurita M, Nishiyama A, Kondo M. Axis-selective photo-Fries rearrangement and photoinduced molecular reorientation in liquid crystalline polymer films. Macromolecules. 2011;44:5736–42.
24. Kubo S, Kumagai M, Kawatsuki N, Nakagawa M. Photoinduced reorientation in thin films of a nematic liquid crystalline polymer anchored to interfaces and enhancement using small liquid crystalline molecules. Langmuir. 2019;35:14222–29.
25. Hasegawa M. Key molecular structure determination of photoalignment materials from the effects of linearly polarized deep UV light on several polymers. Jpn J Appl Phys. 2000;39:1272–77.
26. Usami K, Sakamoto K, Ushioda S. Influence of molecular structure on anisotropic photoinduced decomposition of polyimide molecules. J Appl Phys. 2001;89:5339–42.
27. Du T, Fan F, Tam AMW, Sun J, Chigrinov VG, Kwok HS. Complex nanoscale-ordered liquid crystal polymer film for high transmittance holographic polarizer. Adv Mater. 2015;27:7191–5.
28. Xie X, Du W, Shao Z, Zhou Y, Lou Z, Ji R, Wen D, Wei B, Gan X, Zhao J, Fan F, Tang D. Multichannel binary-image and holographic display based on planar liquid crystal devices. Laser Photon Rev. 2023;17:2300193.
29. Kobashi J, Yoshida H, Ozaki M. Circularly-polarized, semi-transparent and double-sided holograms based on helical photonic structures. Sci Rep. 2017;7:16470.
30. Fukuhara S, Nagano M, Hara T, Seki T. Free-surface molecular command systems for photoalignment of liquid crystalline materials. Nat Commun. 2014;5:3320.
31. Guin T, Settle JM, Kowalski BA, Auguste AD, Beblo RV, Reich GW, White TJ. Layered liquid crystal elastomer actuators. Nat Commun. 2018;9:1.
32. Zeng H, Wani OM, Wasylczyk P, Kaczmarek R, Priimagi A. Self-regulating iris based on light-actuated. Adv Mater. 2017;29: 1701814.
33. Hisano K, Aizawa M, Ishizu M, Kurata Y, Nakano W, Akamatsu N, Barrett CJ, Shishido A. Scanning wave photopolymerization enables dye-free alignment patterning of liquid crystals. Sci Adv. 2017;3:e1701610.
34. Aizawa M, Hisano K, Ishizu M, Akamatsu N, Barrett CJ, Shishido A. Unpolarized light-induced alignment of azobenzene by scanning wave photopolymerization. Polym J. 2018;50:753–59.
35. Aizawa M, Ota M, Hisano K, Akamatsu N, Sasaki T, Barrett CJ, Shishido A. Direct fabrication of a q-plate array by scanning wave photopolymerization. J Opt Soc Am B. 2019;36:D47–51.
36. Hisano K, Ota M, Aizawa M, Akamatsu N, Barrett CJ, Shishido A. Single-step creation of polarization gratings by scanning wave photopolymerization with unpolarized light. J Opt Soc Am B. 2019;36:D112–8.
37. Ueda K, Aizawa M, Shishido A, Vacha M. Real-time molecular-level visualization of mass flow during patterned photopolymerization of liquid-crystalline monomers. NPG Asia Mater. 2021;13:25.
38. Ishizu M, Hisano K, Aizawa M, Barrett CJ, Shishido A. Alignment control of smectic layer structures in liquid-crystalline polymers by photopolymerization with scanned slit light. ACS Appl Mater Interfaces. 2022;14:48143–9.
39. Chigrinov VG, Kozenkov VM, Kwok HS. Photoalignment of liquid crystalline materials: physics and applications. West Sussex (UK): John Wiley & Sons Ltd; 2008. p. 101–35.
40. Kawatsuki N, Norisada H, Yamamoto T, Ono H, Emoto A. Photorefractivity in polymer dissolved liquid crystal composites composed of low-molecular-weight nematic liquid crystals and copolymer comprising mesogenic side groups. Sci Technol Adv Mater. 2005;6:158–64.